International Research Journal of Engineering and Technology (IRJET) e-ISSN: 2395-0056
Volume: 07 Issue: 08 | Aug 2020 www.irjet.net p-ISSN: 2395-0072

Design of 3D Printed Integrated Leg-Flap System and Embedded Control for Amphibious Hexapod with provision for Piezoelectric Energy Harvesting

Nimmagada Sree Nigam Aditya[1], Maheep Bhatt[2], Wedyn Noronha[3]

[1]*School of Mechanical Engineering (SMEC), Vellore Institute of Technology, Chennai, Tamil Nadu, India*
[2]*School of Electrical Engineering (SELECT), Vellore Institute of Technology, Chennai, Tamil Nadu, India*
[3]*School of Mechanical Engineering (SMEC), Vellore Institute of Technology, Chennai, Tamil Nadu, India*

Abstract - *Robots have slowly but surely found their way into various domains. The initiation of this phenomenon was guided by the principle that these technological developments were to be used to simplify human lives, but with time this slowly faded into a concept which replaced humans entirely. At the onset of the 1990s, robots were already replacing factory workers and were used as intelligent tools for completing arduous jobs or those that demanded minimal human error. This paradigm shift brought along with it the age of Autonomous production lines, disaster management robots, drones, humanoids etc. The paper discusses the design of an amphibious robot's limb and it's control system. The robot will be capable of moving on different terrains of mud, sand and water. The limb has been designed on Solidworks and fabricated by Fused Deposition Modeling. The motion is governed by servo motors located on each joint. Systems are in place for obstacle detection and energy harvesting.*

Key Words: *Embedded systems, Additive Manufacturing, Energy Harvesting, Arduino, Amphibious, Robotics, MATLAB, Leg- flaps.*

1. INTRODUCTION

Movement complexity in terrains and unexplored environments pose significant difficulties in exploration of an area. Essentially, robots have to face two common tasks during exploration, namely, walking on the drylands and swimming in water. Thus, Amphibious robots are gaining a lot of traction. They have broad applications in research, resource exploration, disaster management & preventive maintenance to name a few. These robots often employ flipper leg propulsion mechanisms for locomotion. This paper discusses the procedure for the development of an amphibious hexapod that is controlled by embedded systems. The limb's structure has been designed on Solidworks 2018. And can be manufactured by 3D Printing. The limb is fabricated from Polypropylene filaments. The Fused Deposition Modeling (FDM) Technique is used since Polypropylene is a thermoplastic. Each limb houses 3 servo motors for motion and a piezoelectric sensor for energy harvesting[2]. Additionally, an Inertial Measurement Unit (MPU9250) is used to maintain the robots orientation and a temperature sensor is used to monitor the setup temperature under service conditions. An ultrasonic sensor, has been used for obstacle avoidance. The subsequent sections enumerate the steps used to design, manufacture and control the robot.

2. Approach

2.1 Manufacturing Process

The Manufacturing process we had in mind was 3D Printing. Fused Deposition Modeling (FDM) is simple to conduct and requires minimal post processing compared to it's counter-parts. FDM is also economic and provides an adequate surface finish for the part in question.

2.1.1 Material Selection

FDM requires thermoplastic filaments as raw materials. The popular materials for making medium strength parts like robot arms are Polylactic Acid (PLA) and Acrylonitrile Butadiene Styrene (ABS), however due to the nature of the robot's service conditions, water resistance was a necessary demand. Polypropylene (PP) is water resistant and is used to make water resistant watch straps and water tight containers.

Table 1 below is a comparison of these three materials.

Table -1: Comparison of ABS, PP and PLA

Property	ABS	PP	PLA
Water Resistant	–	✓	–
Fatigue Resistance	–	✓	–
Heat Resistant	✓	✓	–
Flexible	–	✓	–
Dissolvable	–	–	–
Bed Temperature	95-110^{0}C	85-110^{0}C	45-60^{0}C
Extruder Temperature	220-250^{0}C	220-250^{0}C	190-220^{0}C

Density	1.04g/cm^3	0.9g/cm^3	1.24g/cm^3
Coefficient of Thermal Expansion	90µm/m-^{0}C	150µm/m-^{0}C	68µm/m-^{0}C
Maximum Service Temperature	98^{0}C	100^{0}C	52^{0}C
Durability	8/10	9/10	4/10
Ultimate Strength	40MPa	32MPa	65MPa
Warping	Heavy	Heavy	Heavy
Dimensional Accuracy	Poor	Adequate	Good

PLA has a tendency to succumb to brittle failure and also warp over time when exposed to sunlight. While ABS shrinks leading to dimensional inaccuracy. Narrowing down to PLA and PP we compared some critical properties like, impact strength, heat distortion, percent of elongation, flexural modulus and flexural strength. The following illustration depicts the comparison.

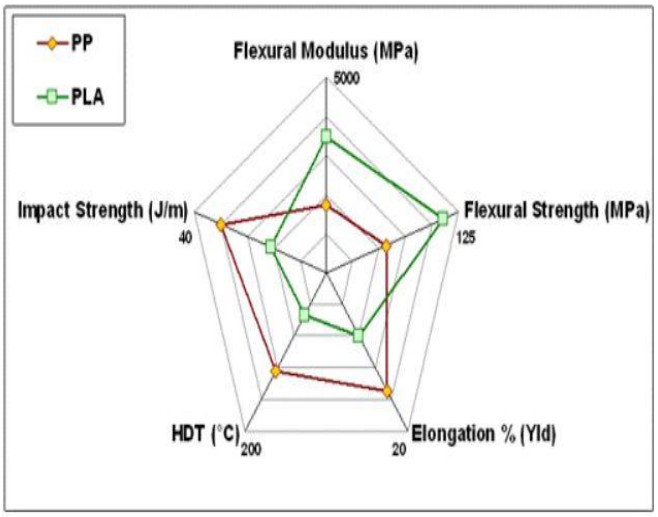

Fig -1: Comparison of Polylactic Acid and Polypropylene

Polypropylene has higher impact strength and has a larger tendency to bend compared to PLA and it can better resist deformation under load. While it has lower flexural strength and flexural modulus because it is more elastic than PLA. PP has a higher heat distortion, thus dimensions could be affected at raised temperatures. Despite it's lower printability, PP was chosen for the following reasons.

- **High impact and fatigue resistance:** The polypropylene is extremely tough and can withstand force and repeated bending without breaking.
- **Increased heat tolerance:** This is useful when employed in barren lands or at surface level of water bodies which is warmer owing to exposure to sunlight.
- **Smooth surface finish:** Most filaments require post-processing in order to smooth the surface after FDM printing. With polypropylene, prints come out smooth already.

PP is also light weight and shows good fatigue resistance. Switching to Polypropylene is also beneficial for the environment. It produces almost no waste and the parts from PP can be recycled multiple times. PP also has a better strength-to-weight ratio than other similar materials.

2.1.2 Fused Deposition Modeling with Polypropylene

PP warps heavily during 3D printing, this is due to it's semi-crystalline structure as opposed to the amorphous structures of PLA and ABS. The semi-crystalline structure causes the material to cool and heat indefinitely in different directions, resulting in increased stresses within the material that cause warping. The cool air flowing through the higher layers causes contraction.

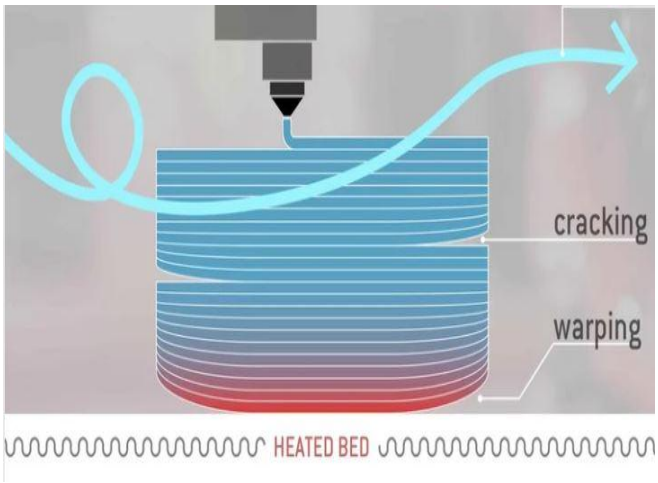

Fig -2: Warping and Cracking

A large brim or raft can be used to increase the surface area of the first layers of the prints, reducing concentrated points of warping stresses. The brim and rafts should be designed such that they snap or peel off after printing. Raising the bed temperature also prevents the layers from cooling down too soon, resulting in lesser contraction. This inhibits the generation of warping stresses. Heated enclosures were useful in maintaining the heat around the print, which reduced contraction considerably. Higher bed temperatures also maintain heat and 85°C is a suitable temperature for PP.

Bed adhesion is also a challenge for printing with PP. Polypropylene adheres well to itself so, polypropylene tapes can be used to facilitate bed adhesion. However, it was observed that polypropylene tapes swelled at temperatures higher than 90 °C.

Print Settings

Bed temperature: 0 – 100 °C
Print temperature: 220-250 °C

Print Speed: 20 mm/s

Number of Layers: $\frac{8\text{mm (part thickness)}}{0.2\text{mm(layer height)}} = 40$;

Filament Diameter: 1.75mm

Extrusion Temperature: 200^{0}C

For 3D prints subjected to low stress, medium strength infill patterns (IP) are used. Infill patterns such as grid, triangles, or tri-hexagon are most appropriate. These patterns however, may increase print time by up to 25%.

Grid: is a 2D pattern that can be printed fast because of it's low complexity.

Triangles: A 2D mesh made of triangles, this pattern has an inherent advantage in strength when a load is applied perpendicular to the object's face. It also makes sense for parts with thin, rectangular components, which might otherwise have very few connections between walls.

Tri-hexagons: This 2D pattern produces hexagons interspersed with triangles. One advantage is that hexagons are an efficient shape, making them a strong infill pattern relative to their material usage. In addition to that, hexagon infill has shorter lines to connect each side, leading to fewer issues with bowing from poor print cooling.

As per findings from "Investigation of infill-patterns on mechanical response of 3D printed poly- lactic-acid" [1] where in a 'Low Velocity Impact' (LVI) test was conducted on Grid, Triangle, Tri-hexagon and Quarter Cubic infill patterns. The objective of the LVI test was to determine the velocity at which the impactor starts to penetrate completely through the material. After penetration of impactor, there will be a residual velocity. The difference between incident velocity and residual velocity will give the penetration limit of each material. A higher amount of penetration of energy could indicate more energy absorption capacity of material during the LVI test which indicates more toughness of the material. The setup for the test consisted of: a clamping bed of adjustable height, a ring fixture, an anti-rebound system, a photo cell sensor, a 20mm hemispherical impactor and a control unit.

The setup is shown below.

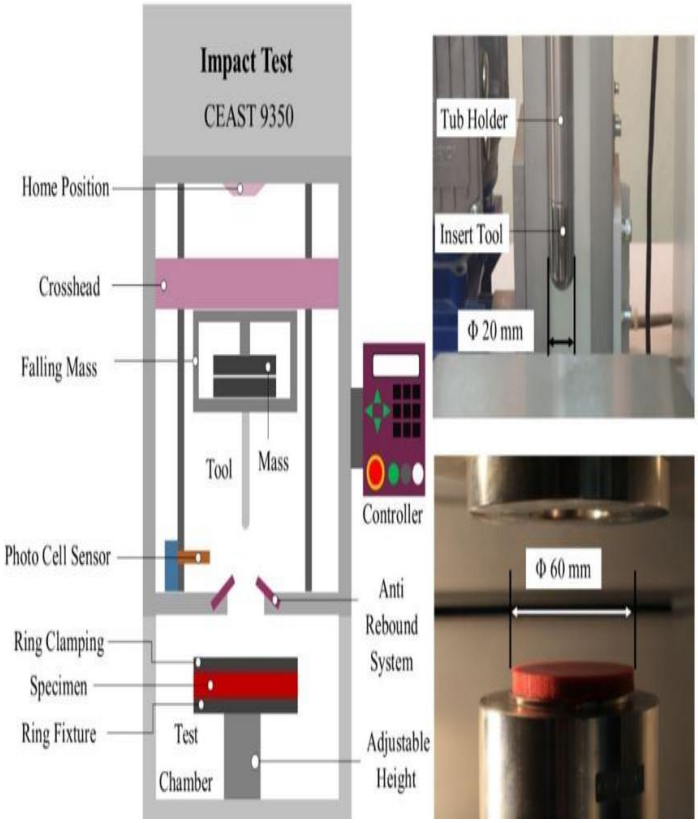

Fig -3: Low Velocity Impact Test Setup

The fixed parameters for the test are tabulated below:

Table -2: LVI Test parameters I

Variable	Selected	Variable	Selected
Filament diameter	1.75 mm	Layer height	200 µm
Platform adhesion type	Brim	Extruder temperature	200 ^{0}C
Nozzle diameter	0.4 mm	Printing speed	20 mm/s
Infill density	60%	Air gap	0
Raster angle	0^0	Heated bed temperature	N/A
No of Extruders	1	No of Layers	40

Table -3: LVI Test parameters II

Parameters	Values, Unit	Parameters	Values, Unit
Input impact energy	50 J	Incident velocity	4.25 m/s
Insert	20 mm	Environmental	25 ^{0}C

diameter		condition	
Falling height	942 mm	Striker load capacity	22 kN

The number of contact points or number of layers where the two layers on the surface level intersect at one point determines the performance on the different infill patterns. The number of contact points per unit area in each infill pattern will define the resistance of the printed specimen against the external load. The figure below shows Scanning Electron Microscope images of the surface topography of the prints with different infill patterns.

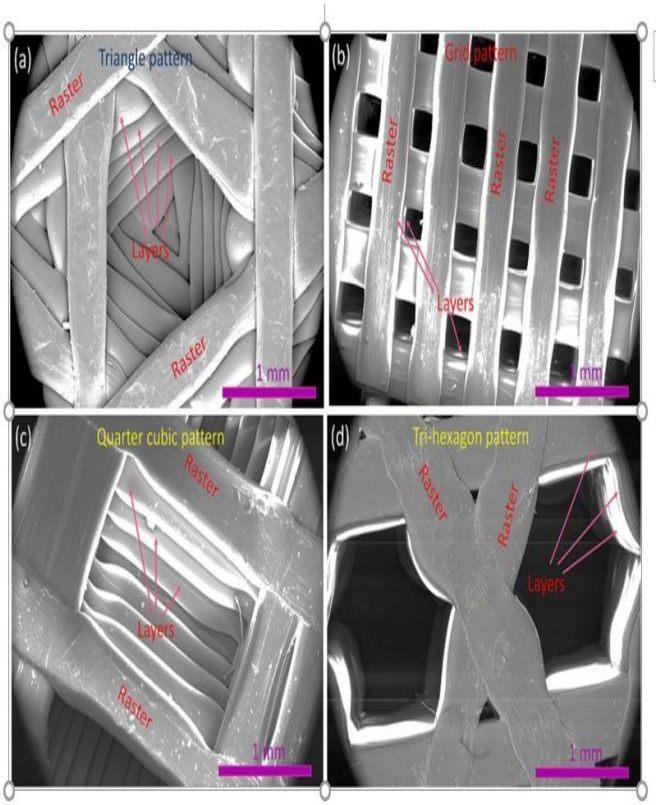

Fig -4: SEM images of surface topography of the infill patterns a) triangle b) Grid c) Quarter Cubic Pattern

d) Tri-Hexagon

Table -4: Impact Properties on Specimens with different infill Patterns

Infill pattern type	Peak force, N	Penetration limit, m/sec	Residual Velocity, m/sec	Penetration acceleration, m/sec^2	Penetration Energy, J	Stiffness, N/mm
Triangle	1190.5	0.28	3.97	107.7	7.5	668.82
Grid	744.4	0.14	4.11	54.54	3.72	547.35
Quarter cubic	1125.1	0.22	4.03	113.04	5.57	557.05
Tri-hexagon	1075.1	0.22	4.03	113.04	5.57	557.05

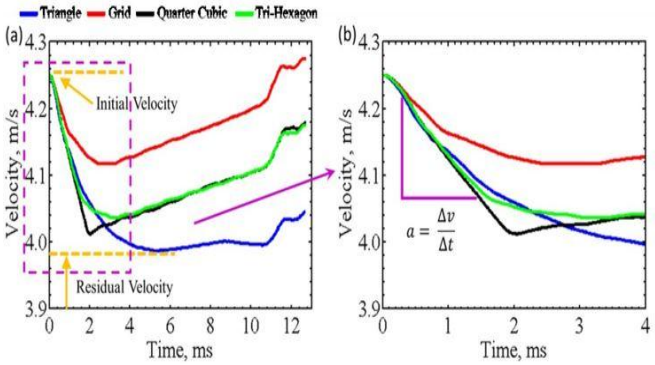

Fig -5: Variation of the velocity-time response of the low-velocity impact test with the function of different IPs; (b) Magnified view showing the calculation of penetration acceleration.

The results show that the triangular pattern has produced the highest absorbed energy in LVI test (penetration energy 7.5 J, and stiffness 668.82 N/mm) because it has more sheared/contact layers' perpendicular to the hemispherical impactor; while the grid pattern exhibited the highest compressive strength (72 MPa) due to more layers aligned along the compressive loading direction. The triangle infill pattern has produced a maximum penetration limit of 0.28 m/s compared to other infill patterns.

Table -5: Results of LVI tests

Infill Pattern Type	No of contact point/sheared points per square mm area	Percentage of sheared area on total
Triangle	9.12	58.41
Grid	5.49	52.49
Quarter Cubic	4.83	39.27
Tri-Hexagon	2.81	39.09

The triangular infill pattern had a higher penetration limit value because it has more contact points/sheared points per unit area (9.12/mm^2) perpendicular to the impactor. Hence, triangular IP has more resistance against the impactor consequently absorbing more energy thus imparting higher toughness and stiffness (668.82 N/mm).

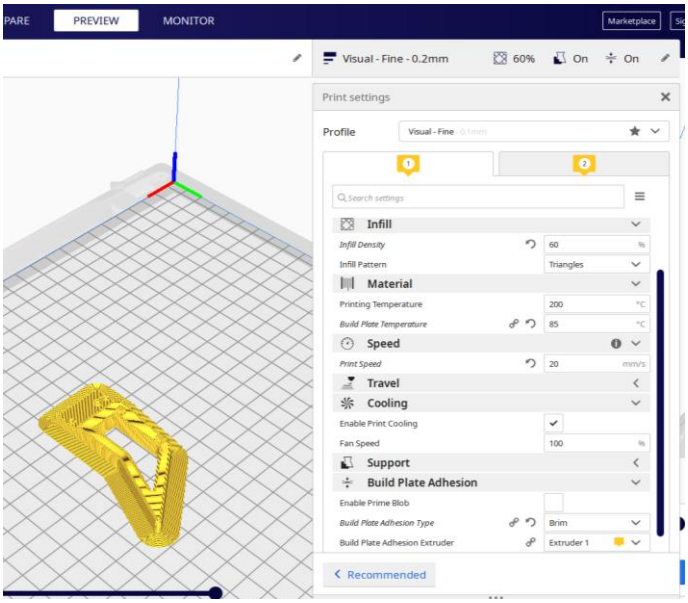

Fig -6: Print Setup in Ultimaker Cura™

2.2 Mechanical Design and Working

The idea of integrated Leg-Flap is inspired by observations from a swimmer's breast stroke. Generally, breast stroke includes initial tearing through the medium by streamlining palms upstream and cup-like formation of the palms for enhancing the thrust developed to propel forwards on the reverse stroke. The flap improves the underwater manoeuvrability of the hexapod by providing the required thrust in specific direction, opening a new horizon for amphibious mobility. The flap system is designed with a self-sensitive mechanical control where in polymeric bevel gears are utilized for perpendicular transmission.

As shown in the following figure, the direction of transmission of the servo motor is changed perpendicularly to power the flap controlling axis. The figure also displays the setup which mirrors the rotational direction on different sides of the leg even while using a single powering source by utilizing the concept of directional change due to orientation of transmission gears.

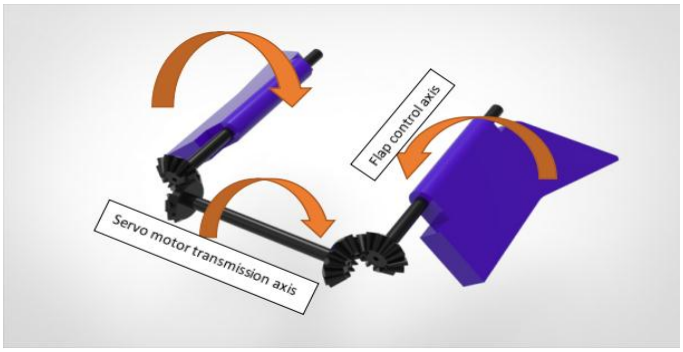

Fig -7: Perpendicular transmission showcasing bevel gears for opposite direction of rotation.

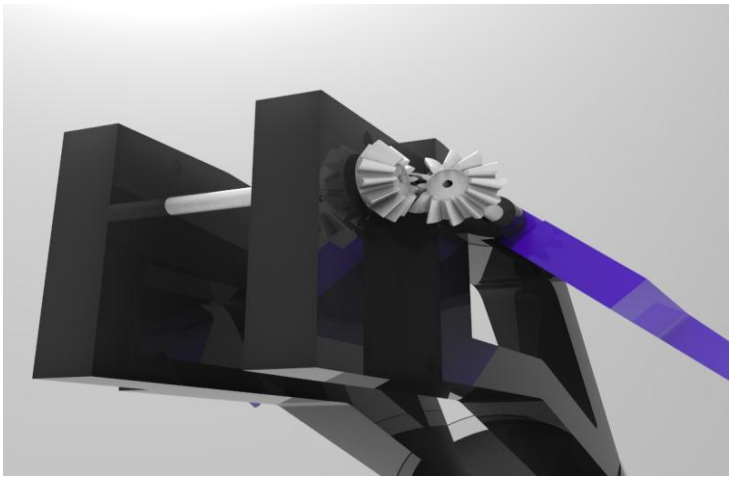

Fig -8: Assembly of the Bevel Mechanism on the leg.

Based on the safe operation range of the Servo motor, the motor is programmed for precise motion. The servo motor opted is programmed for motion of 20 degrees on either side of the neutral position. Here, we can apply the concept of gear reduction in order to obtain desired results. In order to avoid interference between any components the flap is made parallel to the leg I.e 0 degrees with respect to the leg at the point where the servo reaches 20 degrees below the neutral point. For determining the maximum angle for the flap thrust generated on the face of a flap to propel the bot forward is compared. Also, the neutral point of the flap will be half of the maximum angle derived since the servo gives equal deflection on either sides of the neutral point.

Thrust in a fluid medium can be formulated as:

$$Thrust = \Delta P \times A_e$$

Where,

ΔP , is the pressure difference;

A_e , is the effective area generating thrust at different flap orientations.

Considering an ideal situation in mobility, the pressure difference in case of the hexapod's flap will be negligible and directly proportional to the depth of operation of the bot. Hence, the effective area contributes a major part for deriving the thrust generated. The profiles of effective area with respect to change in angle of the flap have been built using CAD models of the prototype design.

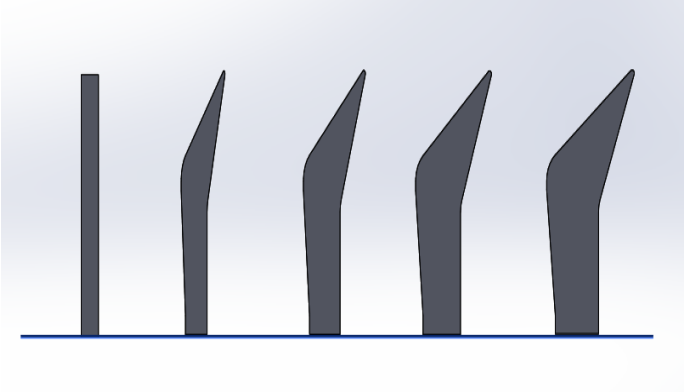

Fig -9: Area profiles generated for different orientations of the flap.

The figure shows the different profiles built for different angles of the flap at discreet intervals. Starting from '0 degrees' at the left to '90 degrees' at the right. The profiles generated had different effective areas and also the design showcases a trend of streamlining of the projected profiles with decrease in angle of the flaps. We can depict from this trend that the profiles at angles below 90 degrees generate lesser aerodynamic resistance in comparison to the apogee at 90 degrees. The data collected has been converted to a graph in order to infer more relevance.

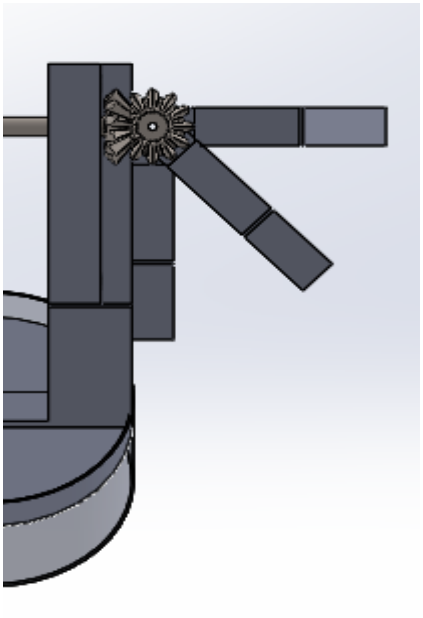

Fig -10: Different angle of the flap as on CAD model.

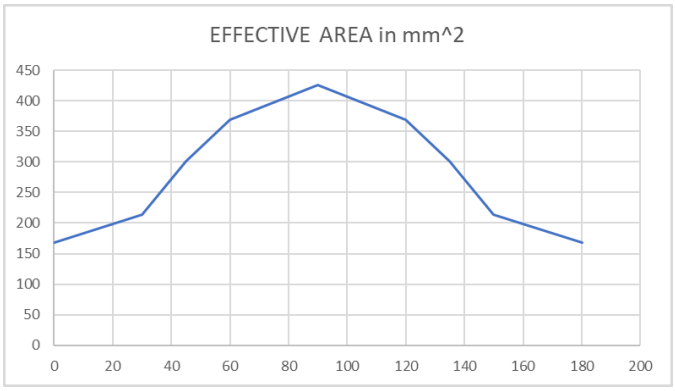

Chart -1: Effective Area in mm^2 vs Orientation of the flap.

From the graph we can derive an inference that the effective area of the flap increases till a maximum at 90 degrees and decreases from there on following a symmetric pattern. Hence, we can decide the maximum angle of the flap to be 90 degrees which draws the maximum thrust.

Since, the maximum of the range of angle of the flap has been determined we can determine the required gear ratio for the bevel gears to create a sound system.

$$GearRatio(G) = \frac{N_{driving}}{N_{driven}}$$

Where,

$N_{driving}$, is the RPM of the driving source i.e the servo motor;

N_{driven}, is the RPM of the driven gear i.e the flap.

Here, the maximum range of the servo motor opted is 40 degrees i.e $1/9^{th}$ of a revolution. Similarly, the desired range of the flap Is 90 degrees i.e $1/4^{th}$ of a revolution. So, we obtain a gear reduction ratio of '4/9' i.e '0.4444' approximately. Further this ratio can be utilized to design the bevel sets with corresponding parameters comprehending the geometric constraints.

Since, Aerodynamic resistance, even though helps generate thrust causes most hindrance to the hexapod, the legs of the bot have been designed to be skeletal in order to mitigate the hindrance by drag. This not only reduces the chance of aerodynamic resistance but also improves the efficiency of mobility due to flap's thrust owing to light weight design.

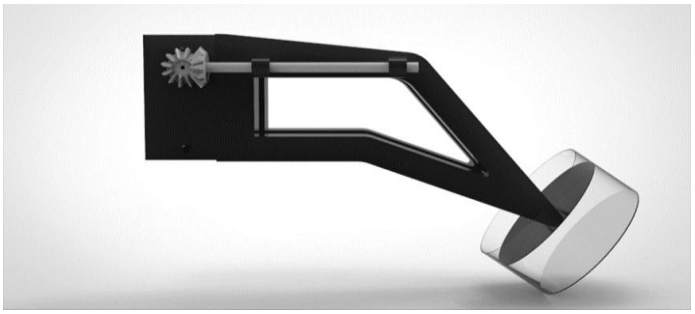

Fig -11: Skeletal design of the leg without the flap.

The figure showcases the provision for mounting the servo motor at the required hinge, also we can see the mounting of the bevel axis using a journal bearing integrated on design.

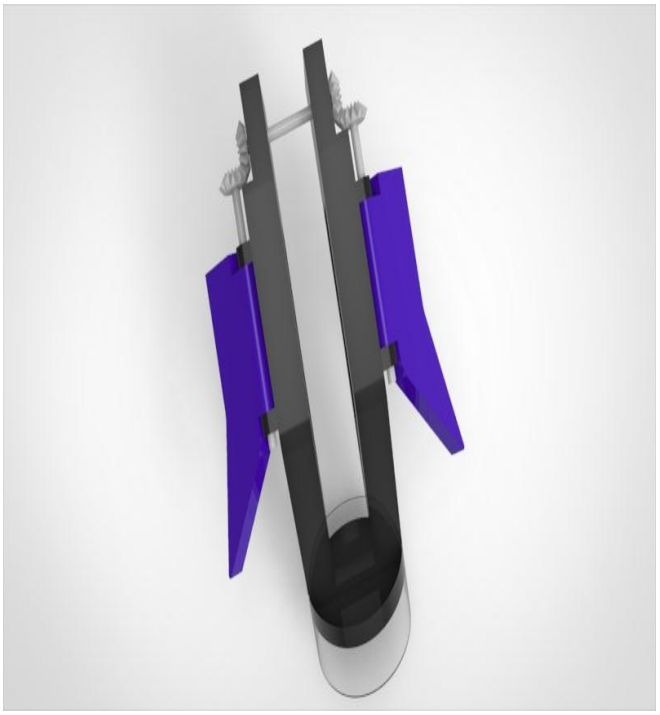

Fig -12: Top View of the final leg design with flaps.

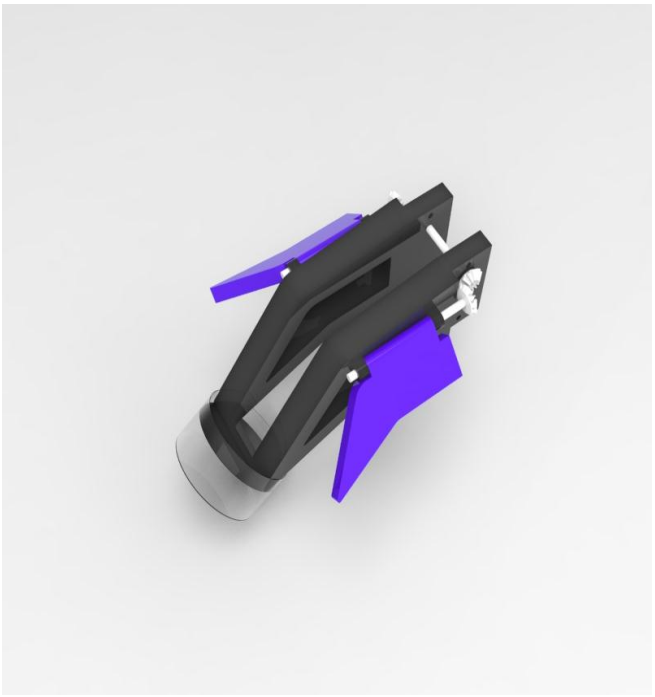

Fig -13: Isometric view of the final leg design with flaps and piezo electric sensor.

The figures show the final design of the integrated leg-flap design along with piezo electric sensor for energy harvesting. The design is minimalistic and skeletal.

2.3 Embedded System

Components used

Arduino Mega 2560*:* This Arduino microcontroller is selected, which is based on Atmega2560; it consists of 16 analog pins, 54 digital I/O pins in which 15 pins are used for Pulse Width Modulation (PWM). It has 5 V operation voltage and around 7-12V input voltage with a recommended clock frequency of 16MHz with a USB connection.

Arduino UNO*:* This microcontroller is based on Atmega328P; it has 14 digital I/O pins in which 6 are PWM pins and 6 analog input pins with an operating voltage of 5 V and 7-12V input voltage with a clock speed of 16 MHz and this also has a USB connection.

Servo Motor*:* Mg996R High Torque Metal Gear Servo Motor is used for the movement of each leg of the hexapod.

Ultrasonic sensor*:* HCSRO4 ultrasonic sensor is used for obstacle detection because it has contactless range detection with high accuracy; its range is 2cm to 400cm.

Inertial Measurement Unit*:* MPU9250 is used for this robot because it straightly provides 9- axis motion fusion output; has a power supply of 3-5 Volts and has both I2C and SPI communication interface.

***Temperature Sensor**:* DHT 22 temperature and humidity sensor are employed because it has a temperature measuring range of -40 to 80 degree Celsius and humidity range of 0-100%.

For energy harvesting, the piezoelectric sensor and rectifier are utilized so that battery which is powering the microcontrollers doesn't drain out and keeps get charging with the movement of the robot.

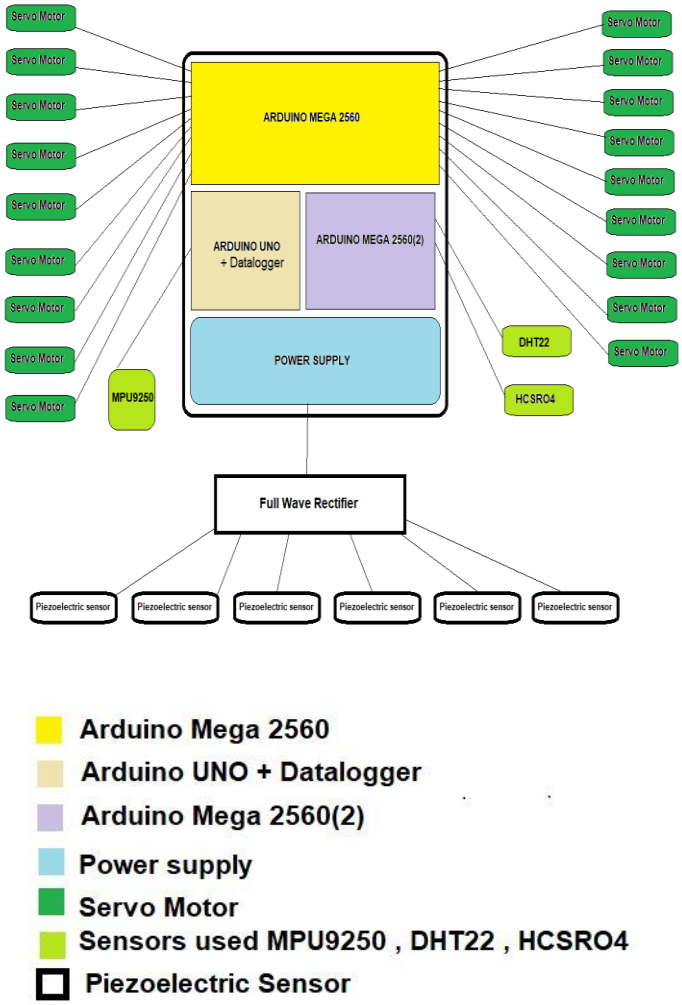

Fig -14: Circuit Diagram

In this robot, each leg has 3 high torque servo motors so total 18 servo motors are used so all the servos are connected to one Arduino Mega 2560 because one Arduino mega has the capacity to control a maximum of 23 servo motors which enables it to calibrate the position of the Centre of Gravity (CG) providing stabler motion while walking.

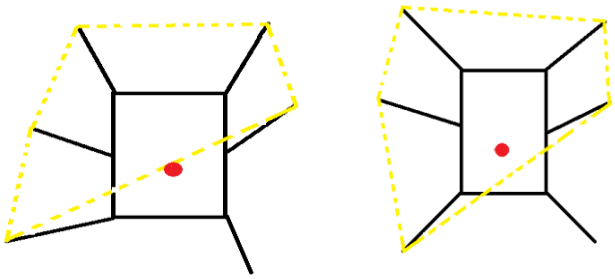

Fig -15: Illustrated calibration for balance based on CG.

So, each leg will have over 30 degrees of flex from the center of gravity so the 5 legs will form a pentagon and the CG should be inside it and the sixth leg is unrestricted and the hexapod will not lose balance. Also, since the pentagon has more potential for positioning the CG than a triangle, it will reduce the chance of tipping over.

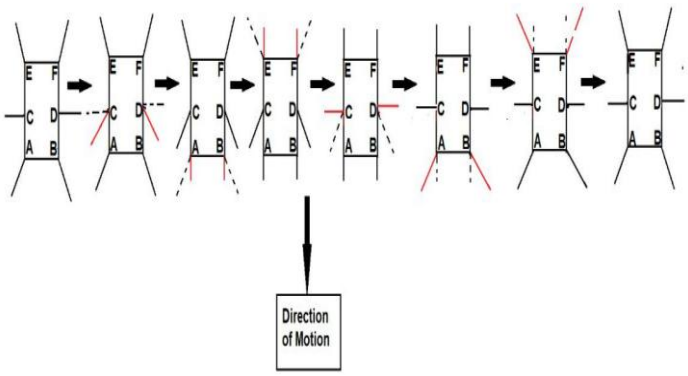

Fig -16: Walking procedure.

Through the initial orientation, four legs(A,B,E &F) in the front and the rear are extended out to the neutral position, and the other two on side(C & D) are actuated forwards as in the figure. Then, the legs 'A & B' are pulled in towards the central axis of the body in the direction of motion, during this actuation the body is balance on the legs 'C, D, E & F'. This is then followed by balancing the bot on the legs 'A, B, C &D' while 'E & F' are actuated to move towards central axis same like 'A & B'. In this section in order to move forward the legs A & B are also actuated to increase the effective length of the leg while E & F are actuated to contract the effective length. This difference in the lengths of the legs is utilized to create a push from the rear legs and pull from the front. This summarizes the basic Walking Protocol followed

by the hexapod, a similar algorithm is applied to control the sideways and reverse motion of the bot.

The temperature sensor is employed in order to measure the setup's temperature when the robot is moving on land as well as when in water. The ultrasonic sensor is used for the obstacle detection and will change its path as per requirement. The IMU gives output in the form of quaternions which are converted to 9 axis data (3 axes each from accelerometer, gyroscope, magnetometer) using Mahoney and Madgwick filter. It collects the data when the robot is being operated and stores it using a data logger in a memory card. After the data is collected, it is processed through Attitude and Heading Reference System (AHRS) filters on MATLAB are used for processing the Inertial measurement unit data which helps us in estimating the orientation of the robot while operation. A complementary filter is deployed as additional provision which processes magnetometer data to enhance the estimation of orientation. As the hexapod is amphibious, in order to make the electrical components water-tight, the motors, sensors and the wiring required has been provided with dedicated 3D printed casings and is sealed off using silicone marine sealant.

The figure below, each leg is fitted with a piezoelectric sensor to harvest energy, which is further utilized to power the bot. Each leg has a telescopic casing compatible with the sensor's constraints and the sensor is actuated when compressed by the weight on the leg, due to this action voltage is generated which then is parsed through a full-wave rectifier as a vibrating piezoelectric sensor produces an AC voltage which is converted to DC voltage. This voltage is stored and used for powering the microcontrollers.

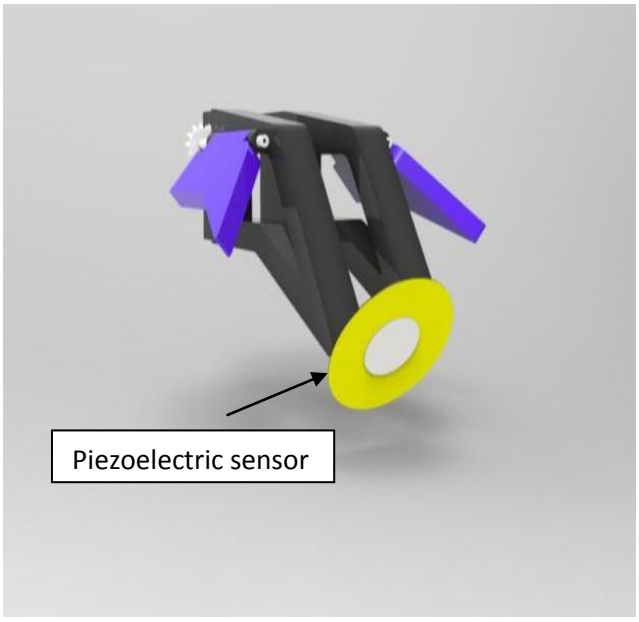

Fig -17: Piezoelectric Sensor

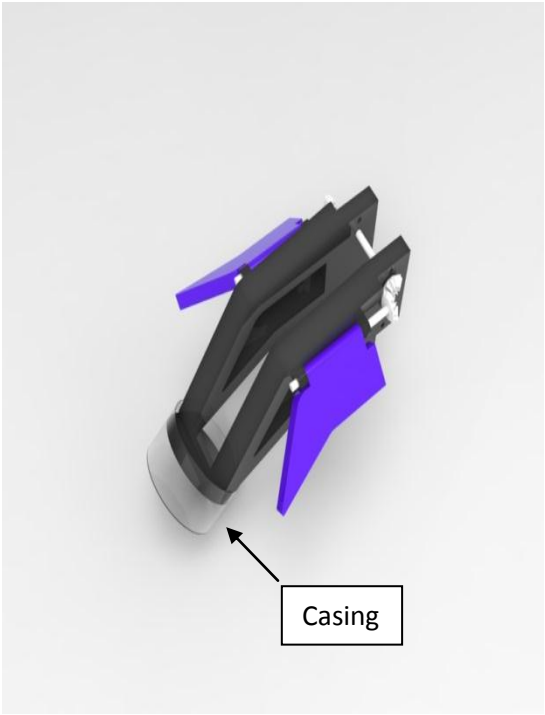

Fig -18: Dedicated Casing

3. CONCLUSIONS

We hypothesize that an amphibious robotic limb can be fabricated using Fused Deposition Modeling, with triangular infill pattern which will project superior impact resistance and high strength. Polypropylene filaments are reliable to fabricate water tight structures that are also durable. In order to enhance the maneuverability of the hexapod the leg-flap has been designed to integrate with the bot. The flap has been designed to generate maximum thrust which can be abstracted adhering to the posed constraints. Subsequently, a self-sensitive mechanical control mechanism for the flaps has been developed which without any external power source will accurately carry out the actuation using bevel sets and precise motion of the opted servo motors. Adequate gear reduction has been provided so as to meet the requirements of the flap design. The design minimizes the aerodynamic resistance and maximizes forward thrust in a fluid medium, bringing meaning to amphibious mobility. The bot is governed by an Arduino-based embedded control system, the system also includes a IMU based data acquisition system which helps user better filter data and understand the preceding data to derive useful terrain results. The hexapod also utilizes a piezoelectric energy harvesting method. This energy is utilized to power the bot.

REFERENCES

[1] Aloyaydi, Bandar & S., Sivasankaran & Alareqi, Ammar. (2020). Investigation of infill-patterns on mechanical response of 3D printed poly-lactic-acid.

Polymer Testing. 87. 10.1016/j.polymertesting.2020.106557.

[2] Lefeuvre, Elie & Badel, Adrien & Richard, Claude & Guyomar, Daniel. (2007). Energy Harvesting Using Piezoelectric Materials: Case of Random Vibrations. J. Electroceram.. 19. 349-355. 10.1007/s10832-007-9051-4.

BIOGRAPHIES

Nimmagadda Sree Nigam Aditya
Head of Technical operations & Head of Manufacturing at University BAJA SAE Team, Suspension Engineer at TSI, Member of SAE INTERNATIONAL, Pursuing B.Tech in Mechanical Engineering at Vellore Institute of Technology, Chennai.

Maheep Bhatt
Head of Electrical Department, of BAJA SAE ATV team, Member of SAE INTERNATIONAL Pursuing B.Tech in electrical and electronics engineering, Vellore Institute of Technology, Chennai..

Wedyn Noronha
Head of Vehicle Dynamics, At BAJA SAE ATV Team Suspension Engineer, Member of SAE INTERNATIONAL Pursuing B.Tech in Mechanical Engineering at Vellore Institute of Technology, Chennai